Communications in Physics, Vol. 32, No. 4 (2022), pp. 389-399
DOI: https://doi.org/10.15625/0868-3166/16829

PYROLYTIC CARBON ELECTRODES AND THEIR POTENTIAL APPLICATION IN ELECTROCHEMICAL SENSORS

NGUYEN THI THANH NGAN[1,†], BUI THANH GIANG[1], NGUYEN DANH THANH[1], NGUYEN DUC THANH[1], NGUYEN HOANG LONG[1], NGUYEN TUAN HONG[2], DANG THANH BINH[2], VU THI THU[1]

[1]*University of Science and Technology of Hanoi, Vietnam Academy of Science and Technology, 18 Hoang Quoc Viet, Cau Giay, Hanoi, Vietnam*

[2]*Center for High Technology Development, Vietnam Academy of Science and Technology, 18 Hoang Quoc Viet, Cau Giay, Hanoi, Vietnam*

E-mail: [†]nguyen-thi-thanh.ngan@usth.edu.vn

Received 14 December 2021
Accepted for publication 4 May 2022
Published 1 October 2022

Abstract. *In this work, pyrolytic carbon electrodes were prepared through pyrolysis of well-patterned AZ 1505 positive photoresist films. The designed electrodes firstly were prepared via photolithography technique, then the polymer was thermally broken-down into carbon skeletons in an oxygen-free environment using pyrolysis technique. The effect of the highest temperature and ramping rate on the electrical properties of the carbon films were investigated. The results show that the pyrolysis process was optimal at the ramping rate of 3°C/minute, annealing temperature of 900°C, and annealing time of one hour. The lowest resistivity was obtained at* 6.3×10^{-5} Ωm *for pyrolytic films prepared at the optimal pyrolysis conditions. Electrochemical measurements confirm the potential of this electrode for electrochemical sensing applications.*

Keywords: pyrolytic carbon; carbon electrodes; electrochemical sensors; pyrolysis.

Classification numbers: 81.05.U; , 82.45.Fk; 82.47.Rs; 82.30.Lp.

I. INTRODUCTION

Carbon-based materials have been widely used in electrochemical sensors due to their outstanding properties such as biocompatibility, inexpensive cost, wide potential window, and electrochemical stability [1–3]. Recently, the electrodes using pyrolytic carbon (PyC) have gained special attention due to their adaptability to manufacture 2D and 3D microelectrodes [4–8]. Besides, it

was reported that the use of PyC might significantly enhance electron transfer at the electrode surface, this improves current responses in electrochemical sensors. These advancements make PyC as a dominant electrode material. Various PyC-based electrochemical sensors have been developed for example water polluted detection, dopamine detection [2, 3], or real-time detection of cell activities [9].

PyC can be simply produced from the pattern of various organic precursors through a carbonization process at high temperatures (750˚C to 2400˚C) in the absence of oxygen molecules [9, 10]. This process is the outgassing of all elements except for carbon and the final structure would contain only carbon. In the first scene, the organic precursor film at around 600˚C generates various hydrocarbon radicals with their highest concentration [11]. At this temperature, the film is also shrinkage due to the outgassing of hydrogen, oxygen, and nitrogen [12]. After approaching 800˚C or higher, the graphene network starts to create in the form of fragments with many defects and impurities [13]. During the annealing time at the highest temperature, the graphene fragments are increased in size while the defects decrease. One of the most important conditions is the absence of oxygen to prevent the burning reaction during the pyrolysis process. Only a very small amount of leaked oxygen can totally decompose the structures and make them unstable. The employing organic precursors are often phenolic resins, polyfurfuryl alcohols, cellulose, and polyimides [14, 15]. The use of positive photoresist AZ1505 as an organic precursor for PyC electrode up to now is limited in previous reports. Especially, AZ1505 is a promising candidate for the two dimension electrodes based PyC due to the easy patterning ability.

This work aims to optimize the pyrolysis conditions (annealing temperature, annealing time, and ramping rate) in order to minimize the resistivity of pyrolytic carbon films based on AZ1505 photoresist. The structural behavior of the materials before and after pyrolysis was tested using Raman and IR spectra. The morphology and thickness of pyrolytic carbon films were examined by Atomic force microscopy (AFM) and Scanning Electron Microscopy (SEM). The electrical conductivity of the films was measured through two-probe method. The effect of the pyrolysis process on swelling effect and improvement in electrical conductivity will also be discussed to evaluate the potential applications of pyrolytic carbon electrodes in electrochemical sensors.

II. EXPERIMENT

II.1. Preparation of un-pyrolyzed polymer-based electrodes

In this study, the using photoresist is AZ1505, a positive photoresist with the ability to fabricate structures with a thickness of around 0.5 μm. AZ1505 also provides some outstanding features such as striation-free coating, low unexposed resist loss, improved adhesion to all common substrate materials. To have the polymer-based electrodes for electrochemical sensing applications, firstly, a thin layer of photoresist was spin-coated onto a clean silicon substrate and soft-baked at 110˚C for 02 minutes to evaporate the solvent in the photoresist. Then the film was exposed to UV light in 3.5 seconds to the bond-breaking reaction occurring through the designed masks. Fig. 1 shows the detail masks with different shapes as well as their dimensions. These designs are appropriate to measure the thin film resistivity.

After being exposed, the samples were hard-baked at 120˚C for 03 minutes and followed by development in AZ developer for 12 seconds, rinsing with water, and drying by Nitrogen gun.

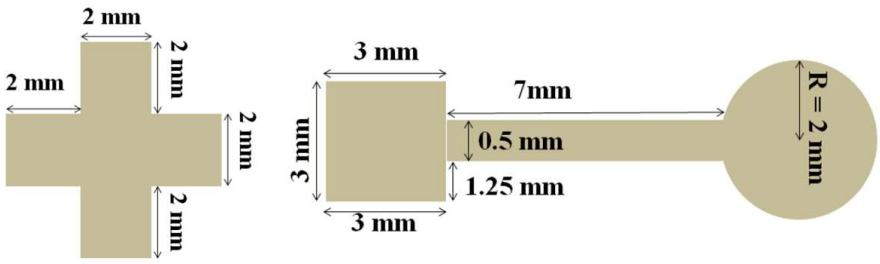

Fig. 1. Electrode designs with different shapes and their dimensions.

The samples were then carbonized by the pyrolysis process which is the thermal decomposition of organic materials at elevated temperatures in an inert atmosphere to expel non-carbon atoms.

II.2. Carbonization of polymer-based electrodes

The carbonization of polymer-based electrodes was carried out in Nabertherm R50/250/12 Compact Tube Furnaces (1200˚C, 250 mm). The samples were loaded into the furnace with an Ar gas flow rate of 300 sccm. The furnace was first heated from room temperature to 200˚C and held for 30 minutes in order to remove the solvent and residual oxygen from the polymer film. Then the temperature was ramped from 200˚C to the highest temperature and remained for 60 minutes to complete the carbonization. Finally, the oven was cooled down naturally to room temperature. The schematic of the whole fabrication process of polymer-based electrodes can be summarized as in Fig. 2.

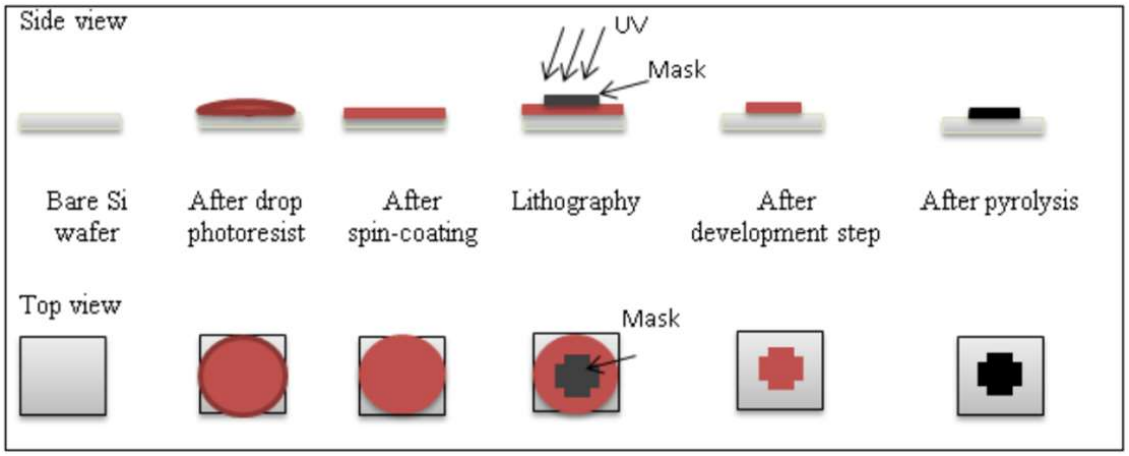

Fig. 2. Schematic of the whole fabrication process.

In this work, the dwell temperatures were studied at different values to evaluate the degree of carbonization. The temperature ramp rate was also investigated with the changing of 1˚C/minute, 3˚C/minute, 5˚C/minute, 7˚C/minute. Fig. 3 illustrates the pyrolysis process with a temperature ramping rate at 3˚C/minute and the carbonization temperature of 900˚C.

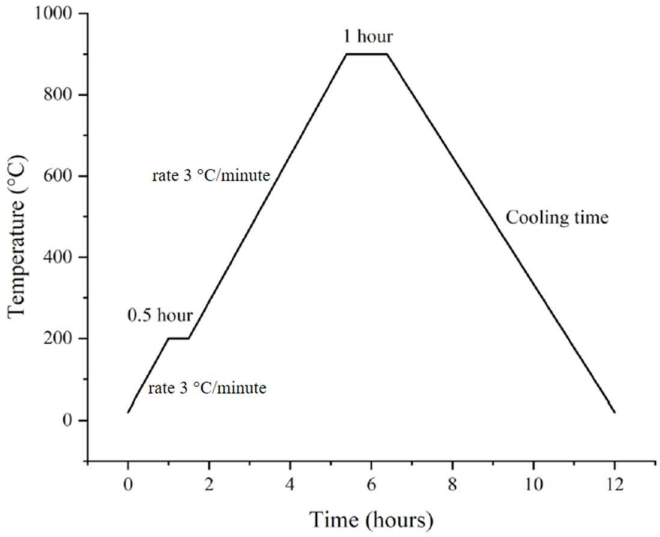

Fig. 3. Schema of pyrolysis process.

II.3. Structural characterization

Atomic force microscopy (AFM) and scanning electron microscopy (SEM) were used to examine the morphology of the synthesized polymer-based electrodes. The components of the film before and after pyrolysis were then investigated by using the Fourier transform infrared spectroscopy (FTIR) measurement. The various peaks related to C-O (900 – 1000 cm^{-1}), C-H (3200 – 3400 cm^{-1}) are expected to exhibit in an organic compound as AZ 1505, while the peaks of C-H in the pyrolytic carbon (carbon film after carbonization) are expected to disappear.

The degree of disorder of pyrolytic carbon (PyC) was characterized by Raman spectroscopy. Normally, Raman spectrum of PyC includes the E_{2g} vibrational mode at 1590 cm^{-1} (also present in graphite) and the A_{1g} vibrational mode at 1360 cm^{-1} [5]. The E_{2g} mode refers to as a "G" peak, where G stands for graphite. The G peak is caused by bond stretching of all sp^2 hybridized C atoms in the aromatic rings as well as in olefinic chains. When the symmetry in the graphite lattice is broken due to the presence of disorder, the A_{1g} mode becomes active. This leads to a new peak close to 1360 cm^{-1}, called the "D" peak, where D stands for disordered. It had been demonstrated that the ratio between the D-peak and the G-peak intensities is reciprocally proportional to the crystalline size La [16]. Hence, the higher the micro-structural disorder of the carbon matrix is, i.e. the higher the number of defects, the higher the D-peak intensity is; therefore, La is smaller [17].

II.4. Measurement of electrical conductivity

The electrical sheet resistance of the PyC film was determined by a two-terminal sensing measurement. The sheet resistance is a special case of resistivity for a uniform sheet thickness and satisfies the equation:

$$R = \frac{\rho}{t}\frac{L}{W} = R_s\frac{L}{W}, \tag{1}$$

where ρ is the resistivity (Ω.m), t is the thickness of the film (μm), R is bulk resistance (Ω), R_s is the sheet resistance (Ω/square), L is the length along the current direction (m), and W is the width of structure (m). After knowing the sheet resistance and the film thickness, the resistivity (ρ) could be calculated using the equation [18]:

$$\rho = R_s t.$$

III. RESULTS AND DISCUSSIONS

III.1. Optimization of pyrolysis process

It is essential to control the pyrolysis conditions to optimize carbonization yield as well as minimize the swelling effect in order to achieve high-quality pyrolytic carbon films [18]. To this end, we have tested the electrical conductivity of the pyrolyzed films at different annealing temperatures (800˚C and 900˚C) and ramping rates (1, 3, 5, 7˚C/minute). The film resistivity was calculated by approximately taking the film thickness at 100 nm.

III.1.1. *Effect of ramping rate*

The effectiveness of the pyrolysis process might be firstly screened by the visual change in color of the polymer film when the temperature ramp rate varies. The highest temperature and the incubation time were maintained at 900˚C and 01 hour. The polymer film is naturally in red color but turned into dark color after pyrolysis process. The color of pyrolyzed film obtained at the heating rate of 3˚C/minute is the darkest, indicating a higher carbonization degree. The measurement of resistivity and sheet resistance with different heating rates which are represented in Table 1 demonstrated for the above hypothesis. It can be seen that, the lower ramping rate, the lower the resistivity or the higher conductivity [16, 19]. However, at the slow flow rate (1˚C/minute) the oxygen in the polymer chain could oxidize the structure leading to the lower carbonization degree [20].

Table 1. The sheet resistance (R_s) and resistivity (ρ) of the samples with different temperature ramping rates.

Ramping rate	$\rho(\Omega m)$	$R_s(\Omega/sq)$
1˚C/minute	3.28×10^{-4}	3.278
3˚C/minute	1.66×10^{-4}	1.661
5˚C/minute	5.29×10^{-4}	5.294
7˚C/minute	22.4×10^{-4}	22.390

III.1.2. *Effect of annealing temperature*

The effect of annealing temperature on electrical conductivity of the pyrolyzed film was given in Table 2. Herein, we kept the ramping rate at 3˚C/minute, the incubation time at 01 hour and changed the dwell temperature at 800˚C and 900˚C. We are not able to test at higher temperatures due to technical issues at our laboratory. However, the results show a significant decrease ($\sim$ 2 times) in resistivity of the film from 3.278×10^{-4} Ωm at 800˚C to 1.661×10^{-4} Ωm at 900˚C. Probably more bindings between non-carbon with carbon atoms have been broken down, thus the carbonization degree was increased at higher temperature [16, 19, 20].

Table 2. The sheet resistance (Rs) and resistivity (ρ) of the samples with different highest temperatures.

Highest temperature	$\rho(\Omega m)$	$R_s(\Omega/sq)$
800˚C	3.28×10^{-4}	3.278
900˚C	1.66×10^{-4}	1.661

III.2. Morphology measurements

The AFM images of the sample before and after pyrolysis are shown in Fig. 4. The optimal pyrolysis conditions were chosen as follows: ramping rate at 3˚C/minute, annealing temperature at 900˚C, and annealing time for 01 hour. The thickness of the polymer film was about 400 nm before pyrolysis (Fig. 4b), and then decreased to 100 nm after pyrolysis (Fig. 4d). SEM image also shows that the thickness of pyrolyzed film was 150 nm (Fig. 5). This dramatically thickness decrease ($\sim$ 4 times) is comparable to previous reports. The reduction might be 48% in curing SU8 precursor [5], or even more than 80% if the maximum pyrolyzed temperature is 1000˚C [8, 9, 21]. The origin of the weight change is still not unclear but it may be due to decomposed reactions of water, oxygen, hydrogen and aromatization [5, 7, 9].

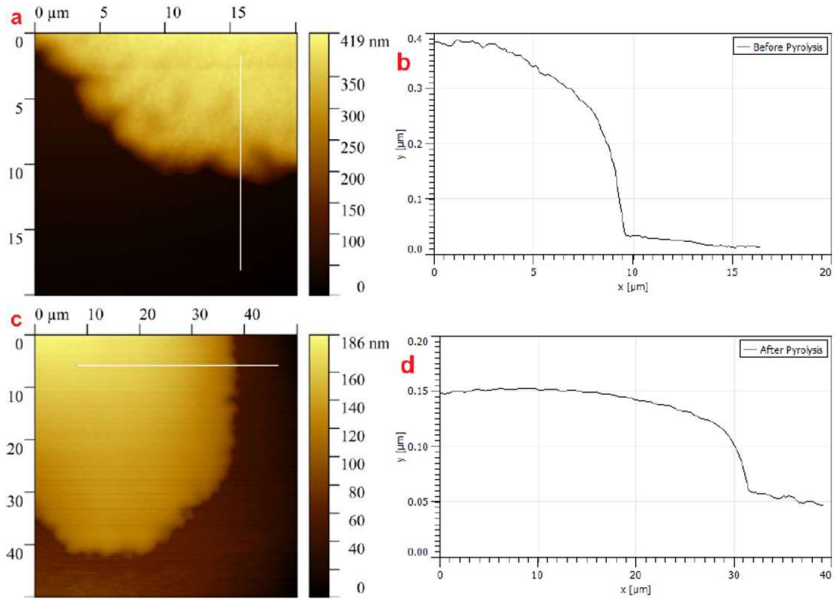

Fig. 4. AFM images (a,c) and extracted line profiles (b,d) of sample before (a,b) and after (c,d) pyrolysis process.

III.3. Structural behaviors of pyrolytic carbon films

Figure 6 shows the FTIR spectra of the sample before and after pyrolysis. The FTIR spectrum of non-pyrolyzed sample consists of several peaks assigned as follows [22-24]: the 3470 cm^{-1} peak corresponds to the OH-stretching vibration of the hydroxyl group; a range of

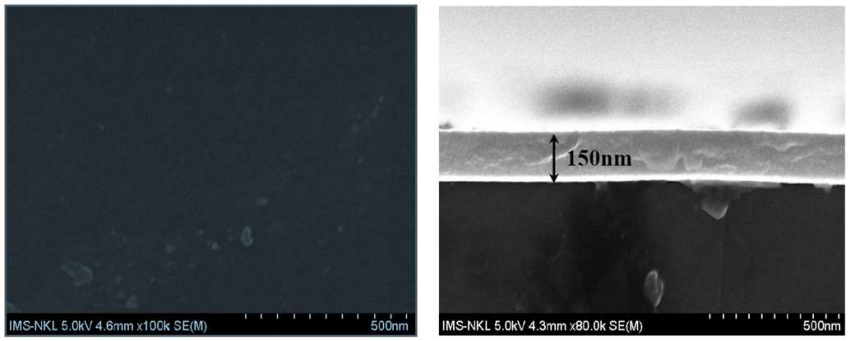

Fig. 5. SEM image of pyrolytic carbon film with temperature ramping rate at 3˚C/min, highest temperature 900˚C, and incubation time for 01h, (left) direct view and (right) side view.

peaks in the region 1200 – 1500 cm^{-1} represents for various C-H vibration of the methyl/methylene group (CH_3/CH_2) or other substances. After pyrolysis, many peaks disappear or strongly decrease, for example, the significant decrease of the OH peak at 3470 cm^{-1}, indicating the success in removing hydrogen out of the structure. In the spectrum of the pyrolyzed sample, a new peak at 1700 cm^{-1} is referred to the C=O stretching vibration of unsaturated carboxyl groups [25]. From the FTIR analysis, it was concluded that pyrolytic carbon is successfully fabricated with a part of the hydroxyl and carboxyl groups on the PyC surface.

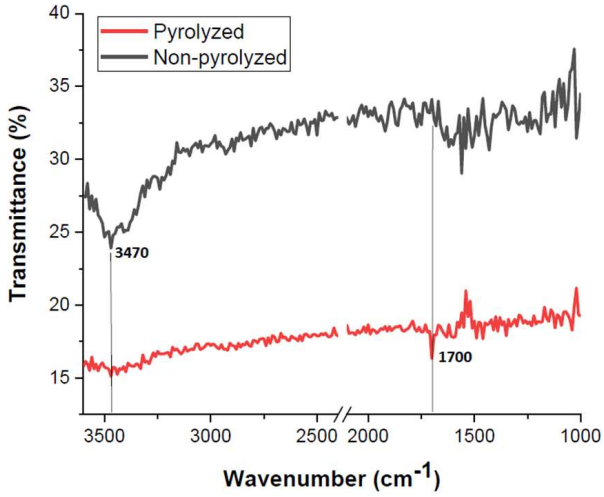

Fig. 6. FTIR spectra of the sample before (non-pyrolyzed) and after pyrolysis (pyrolyzed).

Raman spectrum is also a powerful tool to investigate the quality of the pyrolysis process. Fig. 7 represents the Raman spectrum of polymer-based electrodes after pyrolysis. The pyrolyzed film exhibits a typical graphitic band (G-band) and a defect band (D-band) of carbonaceous materials [5, 18]. The G-band observed at 1598 cm^{-1} is related to E_{2g} vibration mode resulting

from the bond stretching sp^2 hybridized C atoms existing in aromatic rings and olefinic chains of the precursor [4, 19]. The D-band at 1342 cm^{-1} is attributed to the breathing mode of A1g symmetry in sp^2 C atoms and can be used to evaluate the degree of disorder and defects in the lattice [4]. The intensity ratio between D-peak and G-peak is inversely proportional to the crystallite size $La : I_d/I_g \propto La$ [26]. The resulting I_d/I_g ratio after the pyrolysis process is 0.996 which is consistent with results obtained in previously reported works [19, 27], confirming the success of fabricating the pyrolytic carbon.

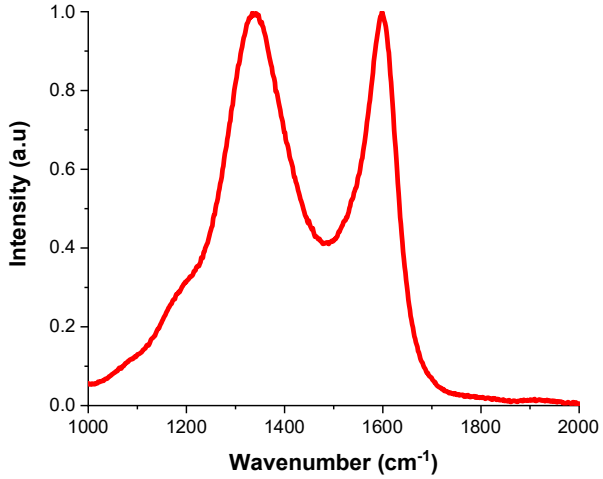

Fig. 7. Raman spectrum of the pyrolyzed film with two characterized peaks of graphite corresponding to D-band and G-band.

III.4. Electrochemical properties

Cyclic voltammetry (CV) experiment which was recorded in the standard redox couple ferri-ferrocyanide, $K_3[Fe(CN)_6]/K_4[Fe(CN)_6]$, solution shows the difference between the film before and after pyrolyzed. As we can be seen, there are no anode and cathode peaks in the non-pyrolyzed CV curve, which means the non-conductive film. It is clear that precursor polymer using is a dielectric material. After pyrolysis, the aromatization and also the dehydrate processes lead to the conductive film with two clearly anode and cathode peaks at -1 V and 1.25 V, respectively. However, the large peak potential separation ($\sim$ 2.5 V) and low currents indicate the slow electron transfer rate [28]. These results represent the suitability of pyrolyzed polymer electrodes in electrochemical applications after optimization of the fabrication process.

Electrochemical impedance spectroscopy (EIS) is an additional tool for evaluation of electrode materials and electrode processes. EIS which is characterized by a large semicircle can yield information about the electron transfer kinetics of the redox system at the electrode interface and thus the electrochemical reaction rate [29–31]. The diameter of this semicircle denotes the charge transfer resistance, Rct. The smaller this diameter value, the lower resistance to charge transfer is. The EIS measurements of the non-pyrolyzed and pyrolyzed films represent in Fig. 9. For the non-pyrolyzed film, the diameter of the semicircle is very large and widens to the higher frequencies range. Besides, the incomplete semicircle implies that there is a non-charge transfer in this case.

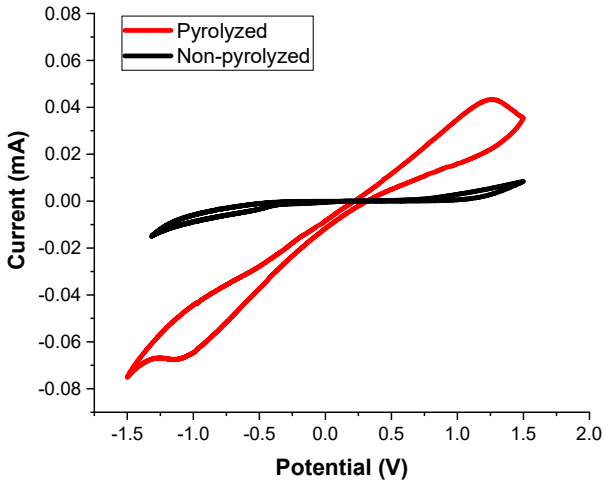

Fig. 8. Electrochemical behavior of non-pyrolyzed and pyrolyzed polymer-based electrodes.

Whereas, the decrease of the semicircle means the decrease of Rct takes place in the pyrolyzed film as illustrated in Fig. 9. The size of the semicircle is rather large ($\sim$ 15 kΩ). This can be suggested that the pyrolyzed process creates the conducting regions ($\sim$ sp^2 regions). However, there are only the patches distributed with insulating areas ($\sim$ sp^3 regions) and thus affected directly to the capacitance of the electrode [4, 32, 33]. This situation can be improved by optimization of pyrolysis parameters.

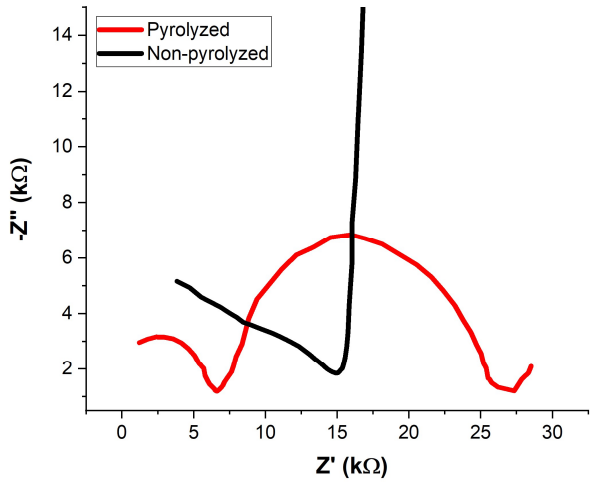

Fig. 9. Nyquist plot for electrode before and after pyrolysis.

IV. CONCLUSIONS

This research was focused on the fabrication and characterization of polymer-based electrodes by photolithography in combination with pyrolysis technique. The effect of pyrolysis process parameters as heating rate and the highest temperature was investigated using SEM, AFM, FTIR, Raman spectroscopy, and two-terminal methods. We see clearly that the heating ramping rate and the highest temperature directly impact the crystallinity and the electrical conductivity of the surveyed samples. To obtain a good quality of carbon structure, the optimized protocol includes the following adjusted parameters: 3˚C/minute of heating ramping rate, 900˚C of highest temperature, and 1 hour of incubation time. The best PyC film obtained has a resistivity of 6.3×10^{-5} Ωm, which is comparable to the reduced graphene oxide and the liquid phase graphene-based film.

The enhancement of the electron transfer effect and also electrochemical properties of the pyrolyzed film compared to the non-pyrolyzed film were also clear from the CV and EIS experiments. Based on these results, we expect that pyrolyzed carbon is an excellent material for electrochemical applications. Further electrode structures such as two-dimension and three-dimension films which are provided a higher electron transfer rate, lower charge transfer resistance, and also larger porosity of surface area will be considered in our next step.

ACKNOWLEDGEMENT

The authors thank the University of Science and Technology of Hanoi (grant number USTH.AMSN.02/21) and Vietnam Academy of Science and Technology (grant number VAST 07.05/21-22) for funding this research. We also would like to express our great thanks to our colleagues at Nano and Energy Center (NEC), Hanoi University of Science for their kindly support in using oven and clean room to conduct the photolithography.

REFERENCES

[1] S. Hemanth, A. Halder, C. Caviglia, Q. Chi, S. S. Keller, *3D carbon microelectrodes with bio-functionalized graphene for electrochemical biosensing*, *Biosensors* **8** (2018) 70.

[2] E. Peltola, J. J. Heikkinen, K. Sovanto, S. Sainio, A. Aarva, S. Franssila, V. Jokinen and T. Laurila, *SU-8 based pyrolytic carbon for the electrochemical detection of dopamine*, https://doi.org/10.1039/C7TB02469J*J. Mater. Chem. B* **5** (2017) 9033.

[3] A. Asif, A. Heiskanen, J. Emneus and S. S. Keller, *Pyrolytic carbon nanograss electrodes for electrochemical detection of dopamine*, *Electrochimica Acta* **379** (2021) 138122.

[4] L. Amato, A. Heiskanen, R. Hansen, L. Gammelgaard, T. Rindzevicius, M. Tenje, J. Emneus and S. S. Keller, *Dense high-aspect ratio 3D carbon pillars on interdigitated microelectrode arrays*, *Carbon* **94** (2015) 792.

[5] S. Hemanth, C. Caviglia and S. S. Keller, *Suspended 3D pyrolytic carbon microelectrodes for electrochemistry*, *Carbon* **121** (2017) 226.

[6] B. C. Benitez, C. Eschenbaum, D. Mager, J. G. Korvink, M. J. Madou, U. Lemmer, I. D. Leon and S. O. Martinez-Chapa, *Pyrolysis-induced shrinking of threedimensional structures fabricated by twophoton polymerization: experiment and theoretical model*, *Microsyst. Nanoeng.* **5** (2019) 38.

[7] I. Mantis, S. Hemanth, C. Caviglia, A. Heiskanen and S. S. Keller, *Suspended highly 3D interdigitated carbon microelectrodes*, **Carbon 179** (2021) 579.

[8] J. A. Lee, S. W. Lee, K-C. Lee, S. I. Park and S. S. Lee, *Fabrication and characterization of freestanding 3D carbon microstructures using multi-exposures and resist pyrolysis*, *Micromech. Microeng.* **18** (2008) 035012.

[9] Y. M. Hassan, L. Massa, C. Caviglia and S. S. Keller, *Electrochemical Monitoring of Saos-2 Cell Differentiation on Pyrolytic Carbon Electrodes*, *Electroanalysis* **31** (2019) 256.

[10] J. Kim, X. Song, K. Kinoshita, M. Madou, R. White, *Electrochemical studies of carbon films from pyrolyzed photoresist*, *J. Electrochem. Soc.* **145** (1998) 2314.
[11] K. Jurkiewicz, M. Pawlyta, D. Zygadlo, D. Chrobak, S. Duber, R. Wrzalik, A. Ratuszna and A. Burian, *Evolution of glassy carbon under heat treatment: correlation structure–mechanical properties*, *J. Mater. Sci.* **53** (2018) 3509.
[12] Swati Sharma, A. M. Rostas, L. Bordonali, N. MacKinnon, S. Weber and J. G. Korvink, *Micro and nano patternable magnetic carbon*, *J. Appl. Phys.* **120** (2016) 235107.
[13] R. Natu, M. Islam, J. Gilmore and R. Martinez-Duarte, *Shrinkage of SU-8 microstructures during carbonization*, *J. Anal. Appl. Pyrolysis.* **131** (2018) 17.
[14] S. Sharma, *Glassy carbon: A promising material for micro- and nanomanufacturing*, *Materials* 11 (2018) 1857.
[15] A. B. Fuertes, I. Menendez, *Separation of hydrocarbon gas mixtures using phenolic resin-based carbon membranes*, *Sep. Purif. Technol.* **28** (2002) 29.
[16] H. Wang and J. Yao, *Use of poly(furfuryl alcohol) in the fabrication of nanostructured carbons and nanocomposites*, *Ind. Eng. Chem. Res.* **45** (2006) 6393.
[17] Y. M. Hassan, C. Caviglia, S. Hemanth, D. M. A. Mackenzie, T. S. Alstrom, D. H. Petersen, High temperature SU-8 pyrolysis for fabrication of carbon electrodes, *J. Anal. Appl. Pyrolysis.* **125** (2017) 91.
[18] L. Amato, K. Schulte, a. Heiskanen, S. S. Keller, S. Ndoni and J. Emneus, *Novel nanostructured electrodes obtained by pyrolysis of composite polymeric materials*, *Electroanalysis* **27** (2015) 1544.
[19] N. McEvoy, N. Peltekis, S. Kumar, E. Rezvani, H. Nolan, G. P. Keeley, W. J. Blau and G. S. Duesberg, *Synthesis and analysis of thin conducting pyrolytic carbon films*, *Carbon* **50** (2012) 1216.
[20] B. Pramanick, M. Vazquez-Pinon, A. Torres-Castro, S. O. Martinez-Chapa and M. Madou, *Effect of pyrolysis process parameters on electrical, physical, chemical and electro-chemical properties of SU-8-derived carbon structures fabricated using the C-MEMS process*, *Mater. Today: Proc.* **5** (2018) 9669.
[21] A. Singh, J. Jayaram, M. Madou, S. Akbar, Pyrolysis of Negative Photoresists to Fabricate Carbon Structures for Microelectromechanical Systems and Electrochemical Applications, *J. Electrochem. Soc.* **149** (2002) E78.
[22] B. Hsia, M. S. Kim, M. Vincent, C. Carraro and R. Maboudian, *Photoresist-derived porous carbon for on-chip micro-supercapacitors*, *Carbon* **57** (2013) 395.
[23] S. Theodoropoulou, D. Papadimitriou, I. Zoumpoulakis and J. Simitzis, *Structural and optical characterization of pyrolytic carbon derived from novolac resin*, *Anal. Bioanal. Chem.* **379** (2004) 788.
[24] S. U. Rege and R. T. Yang, *A novel FTIR method for studying mixed gas adsorption at low concentrations: H_2O and CO_2 on NaX zeolite and γ-alumina*, *Chemical engineering science* **56** (2001) 3781.
[25] B. C. Smith, "Spectroscopy," 01 01 2016. [Online]. Available: https://www.spectroscopyonline.com/view/process-successful-infrared-spectral-interpretation.
[26] Y. Zhang, Q. Cheng, D. Wang, D. Xia. X. Zheng, Z. Li and J. Y. Hwang, *Preparation of pyrolytic carbon from waste tires for methylene blue adsorption*, *JOM* **71** (2019) 3658.
[27] P. Puech, M. Kandara, G. Paredes, L. Moulin, E. Weiss-Hortala, A. Kundu, N. Ratel-Ramond, J. M. Plewa, R. Pellenq and M. Monthioux, *Analyzing the raman spectra of graphenic carbon materials from kerogens to nanotubes: what type of information can be extracted from defect bands?*, *C***5** (2019) 69.
[28] R. Kostecki, B. Schnyder, D. Alliata, X. Song, K. Kinoshita, R. Kotz, Surface studies of carbon films from pyrolyzed photoresist, *Thin Solid Films* **396** (2001) 36.
[29] L. N. Quang, A. Halder, B. Rezaei, P. E. Larsen, Y. Sun, A. Boisen and S. S. Keller, *Electrochemical pyrolytic carbon resonators for mass sensing on electrodeposited polymers*, *Micro and Nano Engineering* **2** (2019) 64.
[30] J. F. S. Pereira, R. G. Rocha. S. V. F. Castro, A. F. Joao, P. H. S. Borges, D. P. Rocha, A. Siervo, E. M. Richter, E. Nossol, R. V. Gelamo and R. A. A. Munoz, *Reactive oxygen plasma treatment of 3D-printed carbon electrodes towards high-performance electrochemical sensors*, *Sens. Actuators B Chem.* **347** (2021) 130651.
[31] G. Gao, L. Z. Cheong, D. Wang, C. Shen, *Pyrolytic carbon derived from spent coffee grounds as anode for sodium-ion batteries*, *Carbon Resour. Convers.* **1** (2018) 104.
[32] B. Rezaei, J. Y. Pan, C. Gundlach and S. S. Keller, *Highly structured 3D pyrolytic carbon electrodes derived from additive manufacturing technology*, *Mater. Design* **193** (2020) 108834.
[33] S. Kwon, H. J. Choi, H. C. Shim, Y. Yoon, J. Ahn, H. Lim, G. Kim, K. B. Choi and J. Lee, *Hierarchically Porous, Laser-Pyrolyzed Carbon Electrode from Black Photoresist for On-Chip Microsupercapacitors*, *Nanomaterials* **11** (2021) 2828.